Electrochimica Acta 512 (2025) 145474

Contents lists available at ScienceDirect

Electrochimica Acta

journal homepage: www.journals.elsevier.com/electrochimica-acta

Reliable testing of acidic OER catalysts in GDE half-cell set-up at industrially-relevant current densities

Timon Elias Günther [a,b,1], Rameshwori Loukrakpam [a,1,*], Bruna Ferreira Gomes [a], Anouk Soisson [a], Melissa Moos [a,c], Bui Duc Long Nguyen [a], Sahil Shah [a], Christina Roth [a]

[a] Electrochemical Process Engineering, University of Bayreuth, Universitätsstraße 30, 95447, Bayreuth, Germany
[b] Department of Resource and Chemical Engineering, Institute for Materials Resource Management, University of Augsburg, Am Technologiezentrum 8, 86159, Augsburg
[c] Department of Ceramic Materials Engineering, University of Bayreuth, Universitätsstraße 30, 95447, Bayreuth, Germany

ARTICLE INFO

Keywords:
PEM water electrolysis
OER performance
Industrially-relevant current densities
Flow field geometries
Gas diffusion layers (GDL)
GDE half-cell setup

ABSTRACT

Production of green hydrogen from acidic and, in the future, alkaline membrane water electrolysers, is an important puzzle piece in our future energy landscape. To make the technology economically viable, novel catalysts are routinely investigated in a small-scale rotating disk electrode electrochemical cell, facing well-known limitations with respect to catalyst layer thickness, 3D porous structure and mass transport during testing. The gas diffusion electrode half-cell set-up is one strategy to remedy these limitations, as it offers testing at industrially relevant current densities in a sample environment mimicking the real electrolyser conditions. Although the GDE half-cell set-up has already been successfully applied in testing of oxygen reduction and carbon dioxide electroreduction catalysts, its application in water electrolysis is still scarce and further insight into the optimal set-up components, robust sample preparation and stable testing conditions is required. In this paper, we aim to elucidate the effect of different flow fields in a gas diffusion half-cell comparing different gas diffusion layers, and reactant feeds during the oxygen evolution reaction in acidic media. In-situ X-ray absorption spectroscopy studies will also be used to unravel the effect of high current densities on the gas diffusion electrodes, which are more realistic towards water electrolyser operations.

1. Introduction

In past years, the development of efficient and durable, mostly noble-metal catalysts has been the focus of research in polymer electrolyte membrane water electrolysis (PEMWE). Iridium and ruthenium oxides were utilised to produce high-purity so-called “green” hydrogen from exclusively renewable energy sources and without CO_2 emissions. And only recently attention shifted towards more earth-abundant catalysts based on Ni, Fe, and Mn, due to the advent of anion exchange membranes, which are finally robust enough to make anion exchange membrane water electrolysis (AEMWE) a viable alternative [1–3].

In common with acidic fuel cells and batteries, the oxygen side in water electrolysers, i.e. the oxygen evolution reaction (OER), is the most demanding reaction, therefore necessitating significant amounts of costly noble metals [4]. Platinum group metals (PGM) like iridium oxide, ruthenium oxide and platinum, already demonstrated their suitability in withstanding the corrosive conditions in PEM electrolysers, with iridium oxides generally showing better stability, whereas ruthenium oxides offer higher OER performance [5–7]. To lower the extensive costs of the green hydrogen technology, a lot of effort is currently being undertaken to reduce the amount of noble metals necessary to sustain the reaction within the porous oxygen-evolving anode [8–10]. Consequently, the design of the porous 3D electrode structure is of utmost importance, as only accessible catalyst material will be utilised effectively, whereas the not conductively connected catalyst fraction will also not be electrochemically addressed [11].

In 2022, the Gasteiger group reported on the durability of porous PEMWE electrodes with significantly reduced iridium content [10]. Herein, they investigated an electrocatalyst concept that would allow for low iridium loadings without decreasing the electrode thickness. Their idea was based on utilising a non-conductive TiO_2 support material, which was then coated with a thin layer of an amorphous hydrous iridium oxide. This approach was very much in line with a recent review paper by Wang and Feng stressing the importance of novel support

* Corresponding author.
E-mail address: rameshwori.jalan@uni-bayreuth.de (R. Loukrakpam).
[1] Equal contribution.

https://doi.org/10.1016/j.electacta.2024.145474
Received 23 July 2024; Received in revised form 5 November 2024; Accepted 2 December 2024
Available online 4 December 2024

materials [12]. Smart support design can be used to increase the number of exposed active sites and take advantage of strong metal-support interactions to increase activity and stability. Also, completely new ways to process porous PEMWE electrodes have been explored recently. In a recent paper by Lee et al. ionomer poisoning effects have been identified as detrimental to the electrode's performance, so that the authors aimed for the direct processing of ionomer-free electrodes. This strategy also offered a more facile recycling route for these less material-complex porous transport electrodes [13,14]. Above exemplary papers have in common that they all highlight the importance of improving the electrocatalysts' intrinsic activity, considering not only the obvious factors, such as structure design, morphology control, and support selection, but also taking into account the performance of electrocatalysts under real-life PEMWE operation conditions. Realistic conditions would include thick and porous catalytic layers, their contact with liquid/gas phase, and their exposure to current densities above 200 mA cm^{-2}, which would all have significant implications on their testing outcome [15].

In the light of the above, it appears that testing of novel catalysts in their powder form in a thin film model rotating disk electrode (RDE) approach might not be sufficient to unravel the effects of operation on the 3D porous catalytic layer in a realistic membrane-electrode assembly (MEA). To characterise such MEAs properly, gas diffusion electrode (GDE) half-cell systems can help to evaluate the catalyst response under realistic operation conditions, as shown for instance by Pinaud et al. and Ehelebe et al. for fuel cell applications [16,17]. Compared to RDE testing in model thin films, the interaction between support material, catalyst/ionomer, membrane and the electrolyte in the so-called triple phase boundary could be probed in depth, and also the impact of the potential-dependently produced gas bubbles (H_2/O_2) and their detachment during water electrolysis considered. In a mini-review by Loukrakpam et al. a comparison between different GDE set-ups for application in fuel cells was provided [18]. The same authors also discussed the application of accelerated stress tests (AST) in this set-up [19]. Similar or slightly modified GDE half-cell set-ups have also been shown to be easily coupled with identical location - transmission electron microscopy (IL-TEM) and X-ray scattering investigations, as has been demonstrated recently by Schröder et al. and Alinejad et al. [20, 21]. A modular, compartmentalised gas diffusion half-cell set up was introduced by Inaba et al. [22], which has the capability of testing low-loaded GDEs and catalyst coated membranes (CCM) in even more realistic conditions at elevated temperatures (up to 60 °C) and using humidified gases with a flow field. Herein, a benchmark carbon-supported Pt nanoparticle (Pt/C) catalyst as well as sputtered model Pt thin films were tested using cyclic voltammetry (CV) or linear sweep voltammetry (LSV) in conjunction with positive feedback for ohmic drop compensation [23].

Pinaud et al. [16] introduced the so-called Staircase Galvano Electrochemical Impedance Spectroscopy (SGEIS) method for acquiring highly precise polarisation curves in such half-cell set-ups. Unlike the typically used CV method involving sweeping the potential by a defined scan rate, the SGEIS is characterised by a staircase-shaped constant current where the potentiostat acts as a galvanostat. To avoid capacitive resistances in the system, which might vary inconsistently during CV measurements, an electrochemical impedance spectroscopy measurement (EIS) is added after each step in order to fully compensate the ohmic drop occurring in the system during the SGEIS measurements. Further the SGEIS method achieves high current densities without mass transport limitations as it allows the system enough time to stabilise at each current step. Ehelebe et al. demonstrated a similar half-cell setup for proton exchange membrane fuel cells (PEMFC), in which the gas flow field and the electrolyte were separated [17]. Likewise, Loukrakpam et al. demonstrated the use of this technique in accelerated stress tests in half-cells [18,19].

One common feature in the gas diffusion electrode half-cell setups reported in literature is the high current densities achieved in the GDEs during such measurements. The surface properties and stability of the catalysts are expected to change quite significantly as compared to low-loading thin films on RDE. X-ray absorption spectroscopy (XAS) is a sensitive technique to study the oxidation states and follow structural changes of catalyst materials and electrodes. Prior XAS operando studies have mostly been performed at the lower end of applied OER potentials, i.e. between 1.2 and 1.5 V vs RHE [6,7]. With increasing potential and current densities above 200 mA cm^{-2}, however, in-situ studies become more demanding due to the high bubble formation rate and the interference of the bubbles with the X-ray beam during the OER reaction when XAS is performed in transmission mode.

In this work, the set-up from Inaba et al. [22] was modified with stainless steel current collectors with a meandering and a parallel flow field for either gaseous or liquid reactant feeds. Application of a flow field helps to avoid gas-liquid mass transport limitations at the high current densities applied during water splitting reactions as reported by Roenning et al., Schroeder et al. and Zhou et al. [24–26]. An ideal flow field should facilitate flow gas/liquid flow stability and have a uniform flow velocity distribution promoting uniform current distribution during water electrolysis reactions. The optimal flow field for water electrolyzers is difficult to pin-point due to lack of optimization of the operational parameters on different flow fields. A study was reported by Yang et al. on four different types of flow fields, namely, parallel, single-channel, four-channel, and parallel grid, and their effect on performance of hydrogen evolution reaction [27]. Herein, an attempt will be made to understand whether the type of flow field will influence the final OER performance in GDE half-cells.

Carbon-supported Iridium (Ir/VC) electrodes with a loading of 1 mg cm^{-2} were prepared on various commercially available gas diffusion layers (GDL) featuring different porous structures: i) carbon paper without a hydrophobic microporous layer (CP), ii) carbon paper with a hydrophobic microporous layer (CP + MPL), and iii) compressible and flexible carbon paper with a hydrophobic microporous layer (CC + MPL). The GDEs were fabricated using a uniform spray-coating technique. Fig. 1 illustrates the differences in the used GDL in more detail. These GDEs were then processed into half-MEA structures (membrane + catalyst layer + GDL) with polymer electrolyte membranes to simulate realistic testing conditions and to access reliable values for OER activity, overpotential, and conductivity due to ionomers and high current density in these GDE half-cell systems [28]. The difference between humidified gas and direct water feed was also evaluated for the GDLs and the two flow fields. In-situ XAS studies further revealed the effect of high current densities on the electrocatalysts subjected to high OER potentials in acidic media, using a GDE half-cell specifically designed for coupling electrochemical performance testing with spectroscopy measurements.

2. Materials and methods

2.1. Materials

2.1.1. Gas diffusion layers (GDLs)

Three commercially available materials were used as gas diffusion layers.

1. Freudenberg H23C8: Compressible and flexible carbon paper with microporous layer (MPL) and 5 % hydrophobic PTFE treatment (CC-MPL).
2. Sigracet 38BC: Carbon paper with microporous layer (MPL) and 5 % hydrophobic PTFE treatment (CP-MPL).
3. Sigracet 29AA: Carbon paper without microporous layer (CP).

2.1.2. Catalyst

A commercial Ir/VC powder from Premetek Co. containing 20 wt.% iridium supported on Vulcan XC-72 was used as the catalyst. Iridium shows one of the highest activities of pure noble metal catalysts for oxygen evolution and is extensively studied, hence, it was selected as

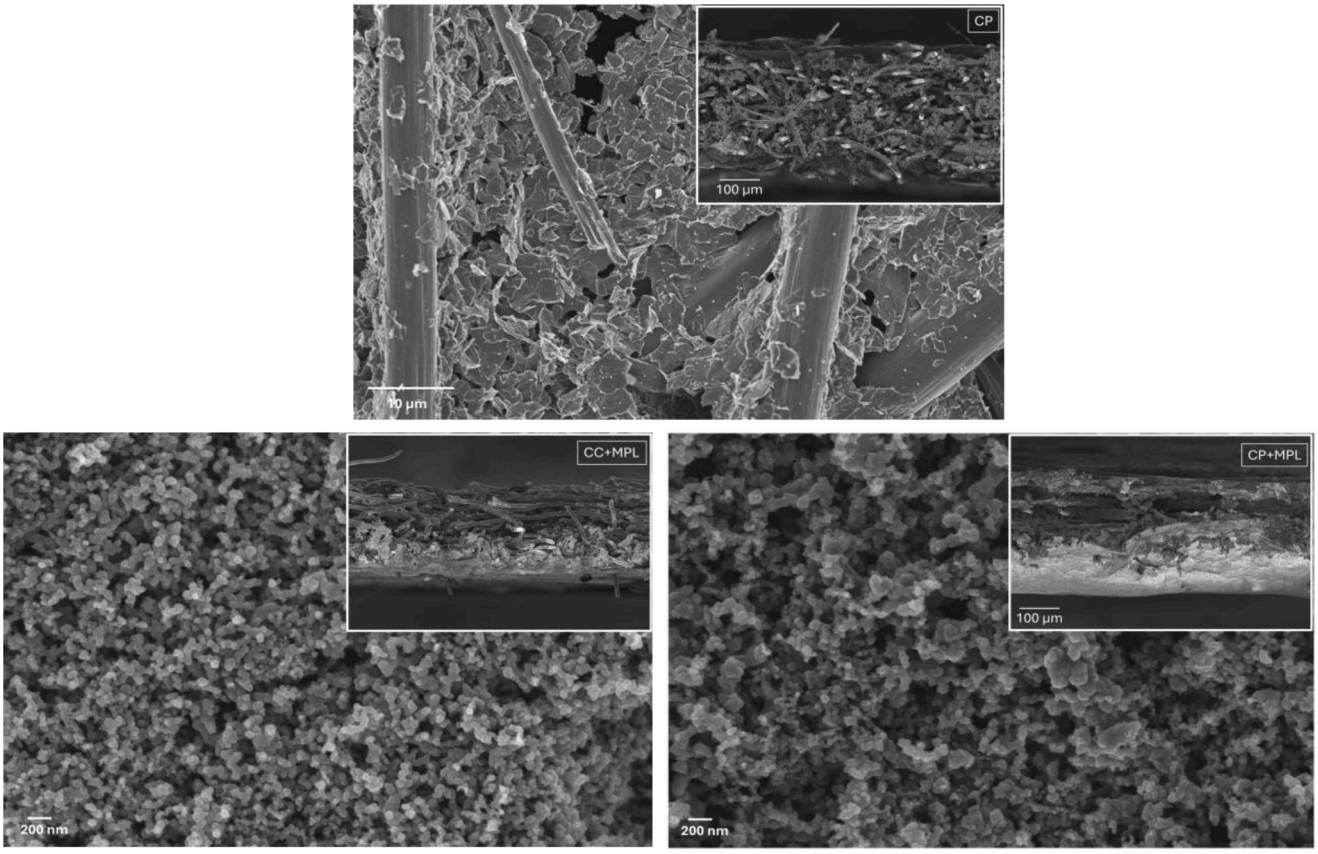

Fig. 1. SEM top view and cross section (inset) of the 3 GDLs.

benchmark material.

2.1.3. Membrane

Perfluorinated sulfonic acid membrane (PFSA), Nafion™ N-117 with a thickness of 183 µm was chosen as laboratory standard. The membrane was pre-treated in 5 wt.% hydrogen peroxide (H_2O_2) for 30 min at 80 °C, then boiled in ultra-pure water (Milli-Q, 18.2 MΩ cm) and activated in 8 wt.% sulfuric acid for 30 min at 80 °C. Finally, they are cut into 20 mm circular pieces and stored in ultra-pure water.

2.1.4. Liquid electrolyte

The liquid electrolyte used for the half-cell testing was 1 M sulfuric acid (H_2SO_4) (ACS Reagent 95 to 97 %). Both sulfate (SO_4^{2-}) and perchlorate ions (ClO_4) are adsorbed on the Ir surface and may have a negative effect on the activity during oxygen evolution. However, Ir is more stable in H_2SO_4 [29].

2.1.5. Ionomer

Nafion solution from Sigma-Aldrich with 10 wt.% was used as binder/ionomer. A nafion layer was applied on top of the catalyst layer and allowed to dry in air. Henceforth, this layer is referred to as "exo-Nafion".

2.2. Experimental methods

2.2.1. Half-cell setup

In addition to a suitable choice of the material and its catalytic properties, the connection and transfer of reactants to and from the gas diffusion electrode are particularly relevant for the scalability of OER electrodes and for the half-cell reaction to occur. Two flow cells with a meandering and a parallel flow field were adapted for the electrochemical measurements [19,20]. The dimension of the flow fields is 1.44 cm^2 for both parallel and single-channel meandering cells. The GDEs hot pressed with membranes were placed on top of the stainless-steel current collector with flow field and covered with a PTFE chamber with an electrolyte volume of up to 25 mL and an exposed electrode diameter of 10 mm (A_{geo} = 0.7854 cm^2). On top of the chamber, a PTFE-cap was placed as holder for the counter electrode (Pt-coil) and a reversible hydrogen electrode (HydroFlex from Gaskatel) (Figure S1 and S2). 1 M H_2SO_4 solution was used as electrolyte at a temperature of 25 °C. All potentials in this paper are reported vs RHE.

2.2.2. Electrode preparation

The GDEs were prepared using spray-coating of the gas diffusion layers (GDL) with an Ir/VC catalyst ink. 300 mg of the Ir/VC was dispersed in 12.7 mL isopropanol and 10 mL ultra-pure water (Milli-Q, 18.2 MΩ cm). 300 mg of 10 wt.% Nafion solution was then added to the ink. To homogeneously distribute the catalyst particles the glass vial with the mixture is placed in an ultrasonic bath (37 kHz, 100 % Power, Elmasonic P) with cold water (< 5 °C) for 45 min. Three different GDLs were used, 29AA (Sigracet), 38BC (Sigracet) and H23C8 (Freudenberg). 5 × 5 cm of the GDL samples were cut and placed on a heating plate at 80 °C to evaporate the solvent mixture during the spraying process. The spray-gun is connected to a N_2 or Ar line with a pressure of 1–2 bar The layer-by-layer spraying of the ink onto the surface needs to be done slowly and in a meandering form to achieve a uniform distribution of the catalyst on the GDL. The catalyst loading of the produced GDE is 1 mg cm^{-2}. Additionally, several layers with 300 mg of 10 wt.% Nafion solution in 10 mL ultra-pure water (Milli-Q, 18.2 MΩ cm) and 10 mL isopropanol can be added onto the sample to achieve better electrical contact of the membrane to the GDL during hot-pressing. This would result in a Nafion loading of 0.025 to 0.05 mg cm^{-2}. After spray-coating, the coated GDLs are cut into circular samples with a diameter of 20 mm and hot-pressed for 2 min at 120 °C.

2.2.3. Electrochemical protocols

Pretreatment: The flow cell is flushed with humidified N_2 at a volumetric flow rate of 100 mL min^{-1} (25 mL min^{-1} liquid water) for 5 min. The catalyst surface was pre-treated by potential cycling between 1.2 and 1.6 V vs. RHE at a scan rate of 200 mV s^{-1} until a stable cyclic voltammogram is recorded (≈ 50 cycles).

OER performance: While purging the flow cell with humidified N_2 at a volumetric flow rate of 100 mL min^{-1} (25 mL min^{-1} liquid water) successive hold currents at 1, 2, 3, 4, 5, 6, 7, 8, 9, 10, 20, 30, 40, 50, 60, 70, 80,90, 100, 125, 150 mA for 2 min each were selected, and the cell voltages recorded using SGEIS. Per current step several data points were generated and averaged over the hold time and each step was iR compensated with EIS recorded on each step.

Chronopotentiometry was performed while purging the flow cell with humidified N_2 at a volumetric flow rate of 100 mL min^{-1} (25 mL min^{-1} liquid water) while a constant electric current of 10 mA was applied for 1 h

For calculation of electrochemical active surface area (ECSA), CVs were performed in the meander flow field half-cell at multiple scan rates in order to measure the double layer capacitance (C_{dl}), in humidified N_2 with a flow rate of 300 mL min^{-1}, in 1 M H_2SO_4 at 25 °C in the non-faradaic region. CVs were measured in the potential window of ± 50 mV centred at the open circuit potential at various scan rates of 2, 4, 6, 8, 10, 25, 50, 100, 200, 400 mV s^{-1}. The ECSA was then derived from the C_{dl} and the specific double layer capacitance (C_s) of the gas diffusion layer with N117 membrane (Figure S3 and S4). The C_s measured was 3 mF cm^{-2} in the 2 to 10 mV s^{-1} range, while it was slightly higher with 4.6 mF cm^{-2} in the 25 to 400 mV s^{-1} range. The C_{dl} measured was 63.8 mF cm^{-2} in the 2 to 10 mV s^{-1} range, while it was slightly higher with 10.5 mF cm^{-2} in the 25 to 400 mV s^{-1} range. Dividing the measured C_{dl} by C_s, an ECSA of 29.2 m^2 g_{Ir}^{-1} was obtained for a GDE with 0.4 mg cm^{-2} Ir loading.

2.2.4. Scanning electron microscopy (SEM)

Scanning electron microscopy (SEM) measurements were carried out by using a Zeiss Ultra plus with a high resolution FEG (field emission gun) scanning electron microscope with 80 mm air lock, inlens SE-detector, chamber SE-detector (Everhart-Thornley), inlens EsB-detector (energy selective backscattered electrons), AsB-detector (angle selective backscattered electrons, 4 quadrants) and STEM-detector (Scanning Transmission Electron Microscopy). The acceleration voltage was 20 kV. There is a gas injection charge compensation system for charging samples as well as a Peltier cooled UltraDry EDS-detector (30 mm^2) and a MagnaRay WDS-spectrometer (both Thermo Fisher Scientific) for elemental analysis. It is also equipped with a Leica cryo system (stage and transfer unit VCT 100) and correlative microscopy (Zeiss Shuttle & Find).

2.2.5. X-ray absorption spectroscopy (XAS)

The in-situ half-cell was composed of a working electrode (GDE), counter electrode (Pt mesh) and a reference electrode (Ag/AgCl, saturated KCl). The electrolyte volume was about 100 mL and N_2 was purged during the measurements. The cell was developed to operate in fluorescence mode to avoid the interference of bubbles with the beam during the OER. Therefore, the back of the GDE (the side without the catalyst layer) was covered with Kapton tape and the electric contact was made using a Pt wire. Then, the GDE was pressed using a PTFE lid against the cell body using a PTFE gasket. The catalyst loading was 1 mg_{Ir} cm^{-2} spray-coated on a GDL, which provided a good signal to noise ratio in fluorescence mode. The cell had a stand that was fixed on the table in order to guarantee that the cell was always in the same position. XAS measurements were performed at P65 beamline at DESY (Petra III, Hamburg, Germany): For each measured potential value, about 4 spectra were obtained (fluorescence mode, PIPS detector) in the region from 11,065 to 12,215 eV (Ir L_3-edge) at different polarisation potentials, with each spectrum being acquired for 240 s. The cell was placed at 45° in relation to the detector (Figure S5). The potentials are reported vs RHE in this paper.

Extended X-Ray Absorption Fine Structure spectra (EXAFS) were normalized in the range between 150 and 1000 eV above the absorption edge using the Athena program [30]. The standardized spectrum was transferred to the SimXLite (software developed at BESSY – KMC3 beamline) program for fitting. The appropriate scattering paths were generated and extracted with FEFF8 software. The fitting was done in k-space and was obtained in the range $\Delta k = 1.60$ to 15.20 $\AA^{-1}$ and $\Delta R =$ 1.0 to 3.0 Å The amplitude factor, S_0^2, was set to 0.7.

3. Results and disussion

3.1. Comparison of the GDLs in humidified N_2 flow and acidic media

Three different GDL types, CP, CP+MPL, CC+MPL (Fig. 1) were spray-coated under sonication with Ir/VC catalysts to produce gas diffusion electrodes with 1 mg cm^{-2} Ir loading. Then, the fabricated electrodes were electrochemically characterised for the oxygen evolution reaction in an applied flow field (either parallel or meander) and in presence of a cation exchange membrane, which combines components of the full fuel cell and the three-electrode setup on a laboratory scale with minimised effort.

By means of the SGEIS method, a polarisation curve was obtained at various current steps with correct iR compensation and the overpotentials were studied using chronopotentiometry under different experimental conditions. The current recorded in the half-cell needs to be normalised either by the geometric area or by using the ECSA based on the Helmholtz double-layer capacitance to obtain the intrinsic activity [31,32]. This is more difficult in Ir catalysts with possible formation of IrO_2 over time, which also do not undergo hydrogen underpotential deposition (H_{upd}) as significantly as Pt catalysts. In electrolytes like H_2SO_4, also anion adsorption needs to be considered, which may additionally block the H_{upd} region. Residual O_2 contained in the electrolyte has also been reported to distort the CVs in the half-cell configuration [31,33,34]. In the results reported below, the current has been normalised using the geometric area. However, it was demonstrated that the ECSA can also be derived using the double layer capacitance measurement method in this half-cell, as detailed and discussed in Figure S3 and S4.

In Fig. 2(a), polarisation curves obtained from the GDEs prepared without an exo-Nafion layer on these three different GDLs in a parallel flow field are depicted. The CC+MPL shows higher current density at the onset, while the current levels off at higher potentials (>1.7 V). CP shows a comparatively slower onset than CC+MPL but is able to sustain high current densities even at higher potentials. The CP+MPL exhibits a delayed onset of OER and is not able to achieve very high current densities compared to the other two GDLs. However, in the meandering flow field as shown in Fig. 2(b), it is clearly evident that the CP performs better than both the other two GDLs with hydrophobic treatment. CP displayed a current density of 25.4 mA cm^{-2} and 22.7 mA cm^{-2} at 1.6 V in meandering and parallel flow fields, respectively. CP+MPL is consistently showing lower current response in either flow fields. At a cell potential of 1.6 V, a current density of 7.6 mA cm^{-2} was measured in parallel flow, compared to 8.9 mA cm^{-2} in the meandering flow. CC+MPL shows a significant difference in the meander flow-field with the slowest onset and lowest current density achieved. Flexible carbon paper with hydrophobic microporous layer (CC+MPL) displayed the highest OER response with current densities of 50.9 mA cm^{-2} under parallel flow, but demonstrated only very low activity in meandering flow with 5.3 mA cm^{-2} at the same corresponding cell potential of 1.6 V.

In Fig. 2(c), polarisation curves obtained from the GDEs prepared with an exo-Nafion layer on these three different GDLs in a parallel flow field are shown. It is clearly evident that the CP and CP+MPL performs better than the CC+MPL with hydrophobic treatment. Similar results to the experiments in parallel flow field were obtained for CP and CP+MPL

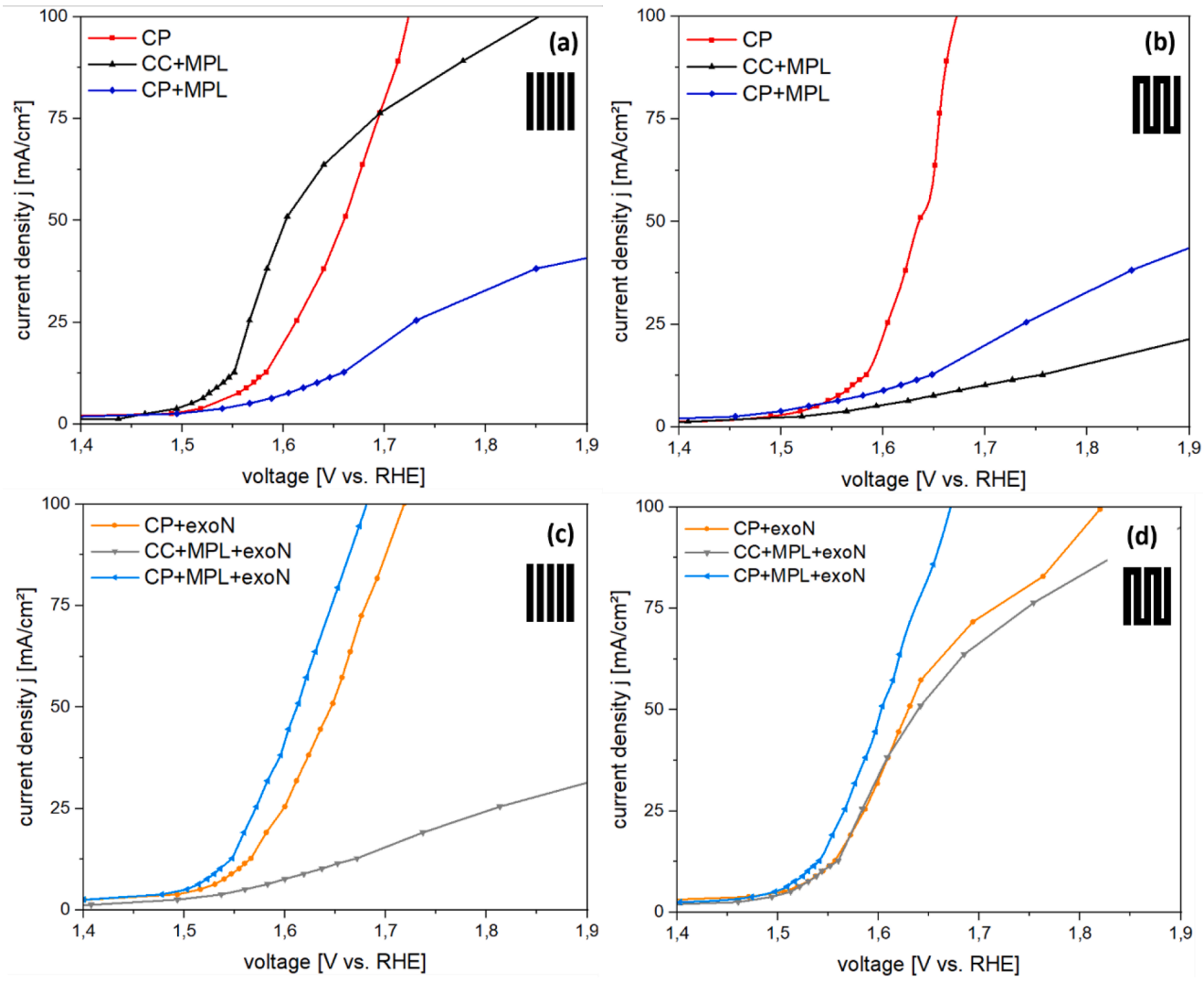

Fig. 2. (a) Polarisation curves for parallel flow on GDEs without exo-Nafion layer; (b) meandering flow field on GDEs without exo-Nafion layer; (c) Polarization curves for parallel flow on GDEs with exo-Nafion layer; and (d) meandering flow field on GDEs with exo-Nafion layer, for OER with N-117 membrane and 1 mg cm^{-2} Ir loading.

in the meandering flow field. The current density measured at a cell potential of 1.6 V for the CP + MPL was 50.9 mA cm^{-2} in the meandering flow field, higher than that in the parallel flow field with 44.5 mA cm^{-2}. A 0.03 V delayed onset was observed for carbon paper without MPL. With the exo-Nafion layer on top, the GDL without microporous layer does not deviate much from the sample with microporous layer. The current densities at the cell voltage of 1.6 V were 25.5 mA cm^{-2} in the meandering flow field and 31.8 mA cm^{-2} in the parallel flow field for CP. Additionally, the OER performance of CC+MPL with exo-Nafion was also enhanced in the meandering flow field, as shown in Fig. 2(d). CC+MPL showed a behavior similar to the other two GDLs in the meandering flow cell with 38.2 mA cm^{-2}, as compared to only 1.6 mA cm^{-2} at 1.6 V in parallel flow field, and thereby demonstrates a behavior that is strongly dependent on the flow field. In contrast to the parallel flow field, CC+MPL showed the expected positive effect of the ionomer layer on the interface between catalyst and membrane in the meandering flow field. Table 1 summarizes the results obtained for the various GDL samples with and without exo-Nafion layer.

The differences between the GDEs with and without exo-Nafion layer are characterized by an early onset potential in the polarization curve and a higher current density at lower cell voltages. The mass transfer is strongly limited in CC+MPL using the parallel flow field and indicates an anisotropy of the carbon fibers in the GDL and dense arrangement of the fibers, which probably is the origin of a different mass transport scenario in the electrode when the current flows in parallel. Comparable interaction of flow field and GDL is reported by Roenning et al. in previous work [25]. The intrinsic structure of the GDL is expected to have a large influence on the electrical contact with any kind of flow field in a PEMWE. Due to the different mechanical flexibility of these three porous structures, the resulting electrical contact with the flow field will also be different. It has been observed by Butsch et al. that carbon paper cannot be strongly pressed against the flow field without losing its structural

Table 1
Comparative performance of the tested GDEs [35,36].

GDL →	CC + MPL	CP + MPL	CP
Ionomer layer (exo-Nafion)	++	++	++
Meander flow	–	++	+
Parallel flow	+	+	+
Hydrophobic treatment	yes	yes	no
Thickness at 0.025 MPa [µm]	230	325	180
Thickness at 1 MPa [µm]	200	280	165
Electrical resistivity at 1 MPa [mΩ cm^2]	<8	<11	<5
Area weight [g m^{-2}]	135	125	32
Compressibility (1 MPa) %	13	14	31

integrity [33]. This could even lead to intrusion of the material and complete blocking of the gas channel within the flow fields and strongly affect the obtained measurement values. Nevertheless, these details need to be considered when devising a reliable testing set-up for water electrolysis in high current density conditions.

Yang et al. reported detailed flow velocity profiles for parallel, single-channel, four-channel, and parallel grid flow fields using three-dimensional (3-D) computational fluid dynamics (CFD) simulations [27]. The parallel and meandering flow fields reported in this study are similar to the parallel and single-channel flow fields reported in the aforementioned article and hence, expected to follow the same flow velocity profiles. The flow velocities at the inlet and outlet were found to be the same in both flow fields. The two different flow path designs exhibited different flow velocities in each channel. In the parallel flow field, the flow velocity was lower in the middle of the flow paths, whereas it was higher in the corners of the flow paths. In the single-channel, fluid velocity was the same in all parts with minor reductions at the channel bends. According to Yang et al. and Duan *et al.*, the flow distribution observed for liquid flow velocities was in the range of 0.1 - 0.5 m s^{-1} [27,37], Wang et al. also reported two innovative structural designs for improved liquid flow uniformity: wedge and rhombus electrolyzers [38].

The CAD-sketches of the two flow fields in this half-cell study were used along with the cross-sectional area and the number of channels to calculate the flow channel coverage area and flow velocities with feed rate of 100 mL min^{-1} (humidified gas flow) and 25 mL min^{-1} (liquid flow). An area of 0.75 cm^2 of the parallel flow and 0.64 cm^2 for the meandering flow are covered by flow channels. During the calculation, we also assume a steady state flow and a single phase in both flow fields. In the parallel flow, the overall flow is distributed towards 13 channels which leads to a different cross sectional-area. Due to this flow distribution, the gas flow velocity is calculated to be 0.45 m s^{-1} in average for the parallel flow field and 1.84 m s^{-1} for the meandering single channel flow field. For liquid water, the flow velocities are found to be 0.11 m s^{-1} in the parallel flow field and 0.46 m s^{-1} in meandering flow. An increase in the number of channels of the single channel flow field is expected to lead to a higher surface coverage of the gas diffusion electrode in laminar flow with increased half-cell performance. A further study involving simulation and optimization of the flow fields for the OER performance can be considered in the future in collaborative efforts with computational groups.

3.1.1. *Chronopotentiometry measurements and TAFEL plots of the OER*

The chronopotentiometry measurements at a constant current of 10 mA with humidified N_2 flowing in both parallel and meandering flow field are shown in Fig. 3. The MEAs with added exo-Nafion layer show significantly lower overpotentials (by around 200 mV) than their counterparts without exo-Nafion. Here, the GDEs with carbon paper (CP and CP+MPL) and exo-Nafion layer show the best results for both flow fields with an overvoltage of 1.54 V to1.6 V. This improvement directly correlates with the early onset potential and higher current density observed for the OER performance at lower potentials. CC+MPL and CP+MPL consistently show higher overpotentials in both flow fields.

Fig. 4 shows the Tafel plots of the GDEs measured and gives an indication of the reaction kinetics towards OER. Among all the GDEs, the highest OER kinetics are demonstrated by CP in the meandering flow field at a Tafel slope of 105.6 mV dec^{-1} and 136.9 mV dec^{-1} under parallel gas flow field. The CC+MPL again shows a strong field-dependent behavior and varies from 121.8 mV dec^{-1} in the parallel flow to 309.3 mV dec^{-1} in meandering flow. Fig. 4(b) and (c) depicts the Tafel plot for the MEA with exo-Nafion layer. Here, the tendency of the improved performance and better kinetics using CP as GDL, independent from the flow field, is confirmed with Tafel slopes varying between 116.8 to 142.4 mV dec^{-1}. Only the flexible carbon paper GDL (CC+MPL) shows a difference in flow field performance improving from 232.5 mV dec^{-1} in parallel flow to 138.1 mV dec^{-1} in meandering flow fields, most likely due to less channel blocking and less hindrance of mass transport by the rather soft/flexible materials intruding less into the meander than into the parallel flow field.

3.1.2. *Flow field comparison with liquid reactant feed*

The OER polarisation curve with liquid water flowing in the half cell was studied only for CP+MPL with exo-Nafion layer in the presence of N117 membrane and is shown in Fig. 5(a). CP+MPL was chosen to also study the liquid in comparison to the gaseous reactant feed as it demonstrated similar performance in both the flow fields when humidified gas was used, as shown in the previous section. The GDE clearly exhibits an early current onset and higher activity in the meandering flow field as compared to the parallel flow field. At a potential of 1.6 V, the current densities obtained for meandering and parallel flow fields differ significantly with 28.6 and 3.0 mA cm^{-2}, respectively. In the meandering flow field, the GDE shows an earlier onset and a sustained OER performance. In contrast, the parallel flow field exhibits sluggish system kinetics, and it seems that the GDE is flooded with reactant,

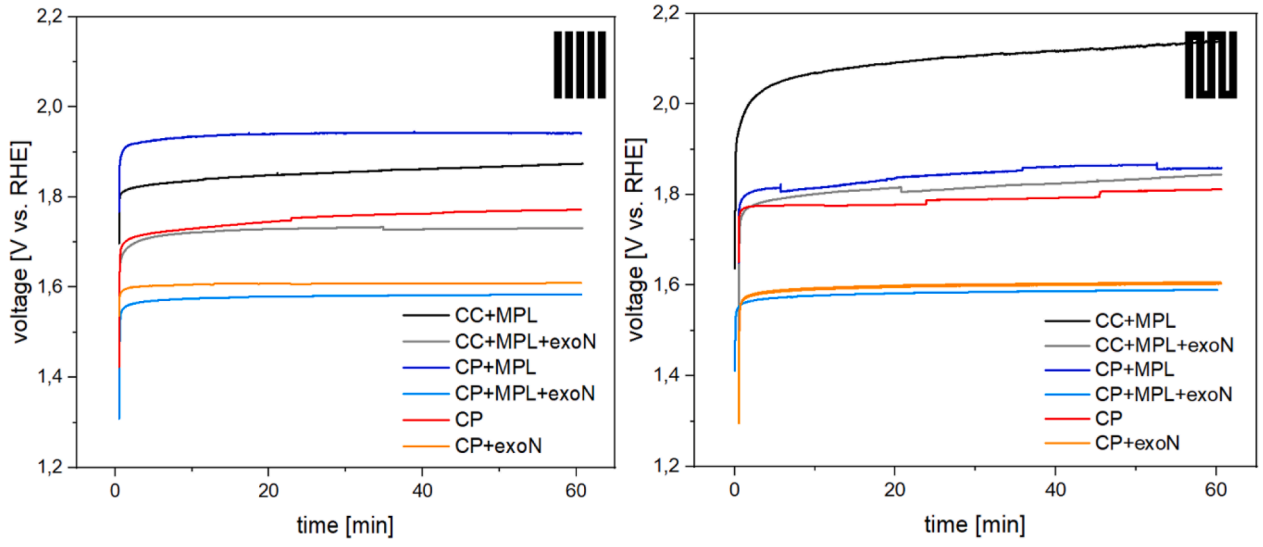

Fig. 3. (a) Chronopotentiometry of the GDEs in parallel flow field and (b) in meander flow field with and without exo-Nafion layer, N-117 membrane, 1 mg cm^{-2} Ir loading, 1 M H_2SO_4.

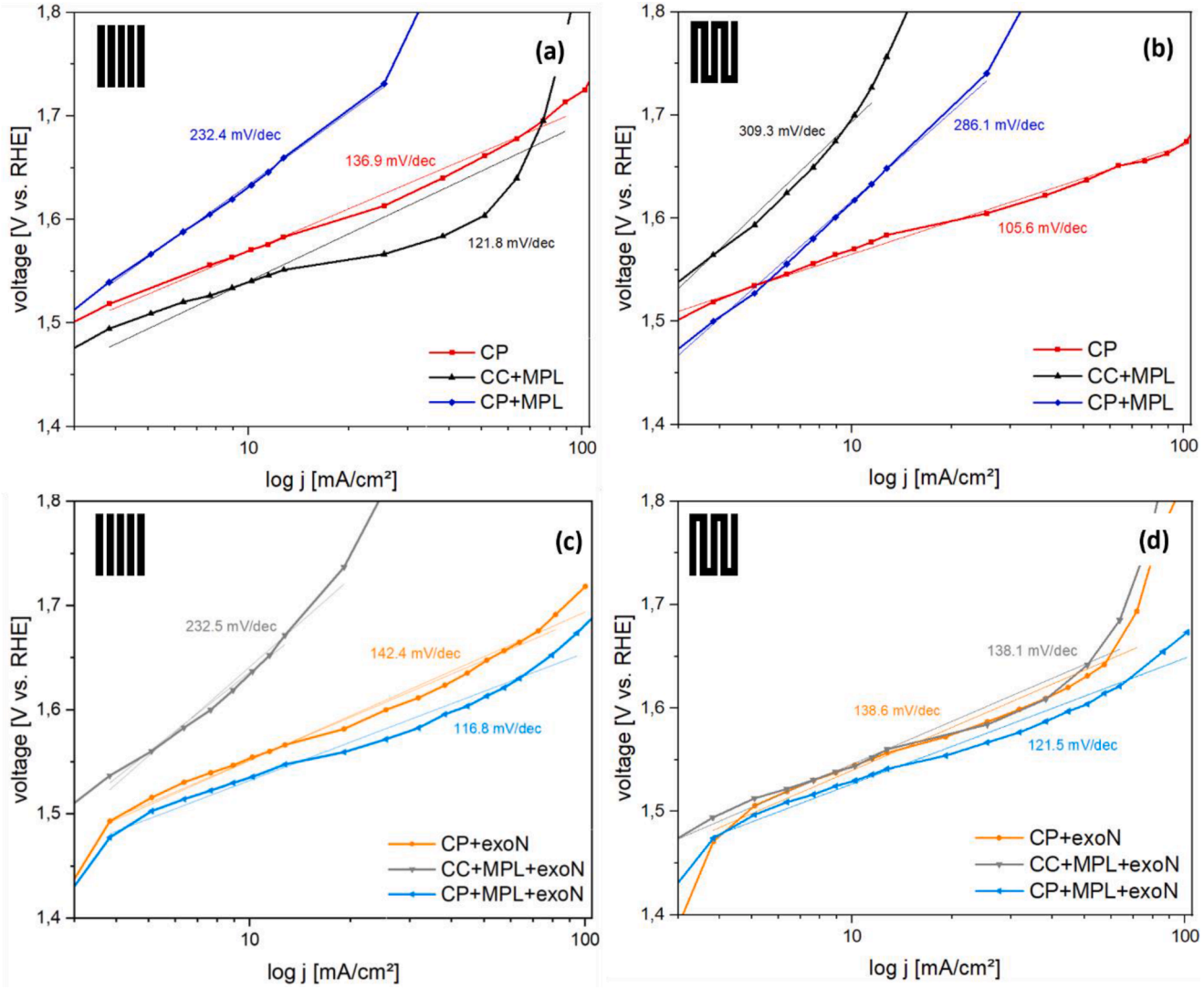

Fig. 4. (a) Tafel plots for parallel flow on GDEs without exo-Nafion layer; (b) meandering flow field on GDEs without exo-Nafion layer; (c) Tafel plots for parallel flow on GDEs with exo-Nafion layer; and (d) meandering flow field on GDEs with exo-Nafion layer, for OER with N-117 membrane and 1 mg cm^{-2} Ir loading.

hence hindering any further increase in current density.

In the chronopotentiometry measurements shown in Fig. 5(b) at 10 mA or 7.6 mA cm^{-2}, a significantly lower and more stable cell voltage over time of 1.57 V was measured for the GDE in the meandering flow field. The result from the parallel flow profile shows a fluctuating cell voltage at the beginning of the measurement, which, however, settles for a constant level of 1.62 V after about 20 min. The Tafel slope of the CP+MPL with liquid flow is the lowest with 98.1 mv dec^{-1}, while the slope in liquid feed was calculated to be 301.6 mV dec^{-1}, as seen in Fig. 5 (c). These results clearly underline the better performance of the meandering flow field in the half-cell as compared to the parallel reactant flow which can flood GDE and hinder further reaction. Fig. 5(d) shows a comparison of all the GDEs studied w/o exo-Nafion layer and the liquid reactant feed in the two flow-fields.

3.1.3. *Overview of the performance of the half-cell*

The measurements in the gas diffusion half-cell setup indicate that the acidic oxygen evolution reaction with a polymer electrolyte membrane still leaves room for improvement in particular with respect to reliability and optimisation. Table 2 gives an overview over the gas diffusion layer performance in different flow fields and helps to weigh the different set-up parameters against each other for the optimisation of the testing set-ups.

With sustained OER activities from the SGEIS measurements and lower overpotential from the chronopotentiometry measurement with 1.57 V in the parallel and 1.62 V in the meandering flow field, carbon paper with a microporous layer was found to be the best performing GDE and optimal for both flow fields. The positive effect of an additional layer of Nafion with a low Nafion loading of 0.025 to 0.05 mg cm^{-2} on the electrode coated with the catalyst material, was evident. The overpotential is lowered by 0.03 to 0.15 V, depending on the GDL used and the effect is independent of the flow field. This exo-Nafion layer improves the adhesion between catalyst and membrane in the gas diffusion electrode during the hot-pressing step and also leads to better proton transport. The best GDE performance is shown in the carbon paper with ionomer layer (CP+exoN) under meandering flow with an overpotential of 282 mV and a Tafel slope of 138.6 mV dec^{-1}, followed by the carbon paper with MPL in the same flow field with 321 and 121.5 mV dec^{-1}. Promising performance was also achieved by the CP with 121.5 and 105.6 mV dec^{-1} in meandering flow field.

The carbon paper without microporous layer showed good suitability for the anodic reaction in both flow fields. With regard to the flow profile, no general statement can be made as to which flow field is the most suitable and is very much dependent on the kind of GDL utilised and the chosen electrode preparation method. The GDEs from the flexible carbon show a clearly better OER performance in the parallel flow

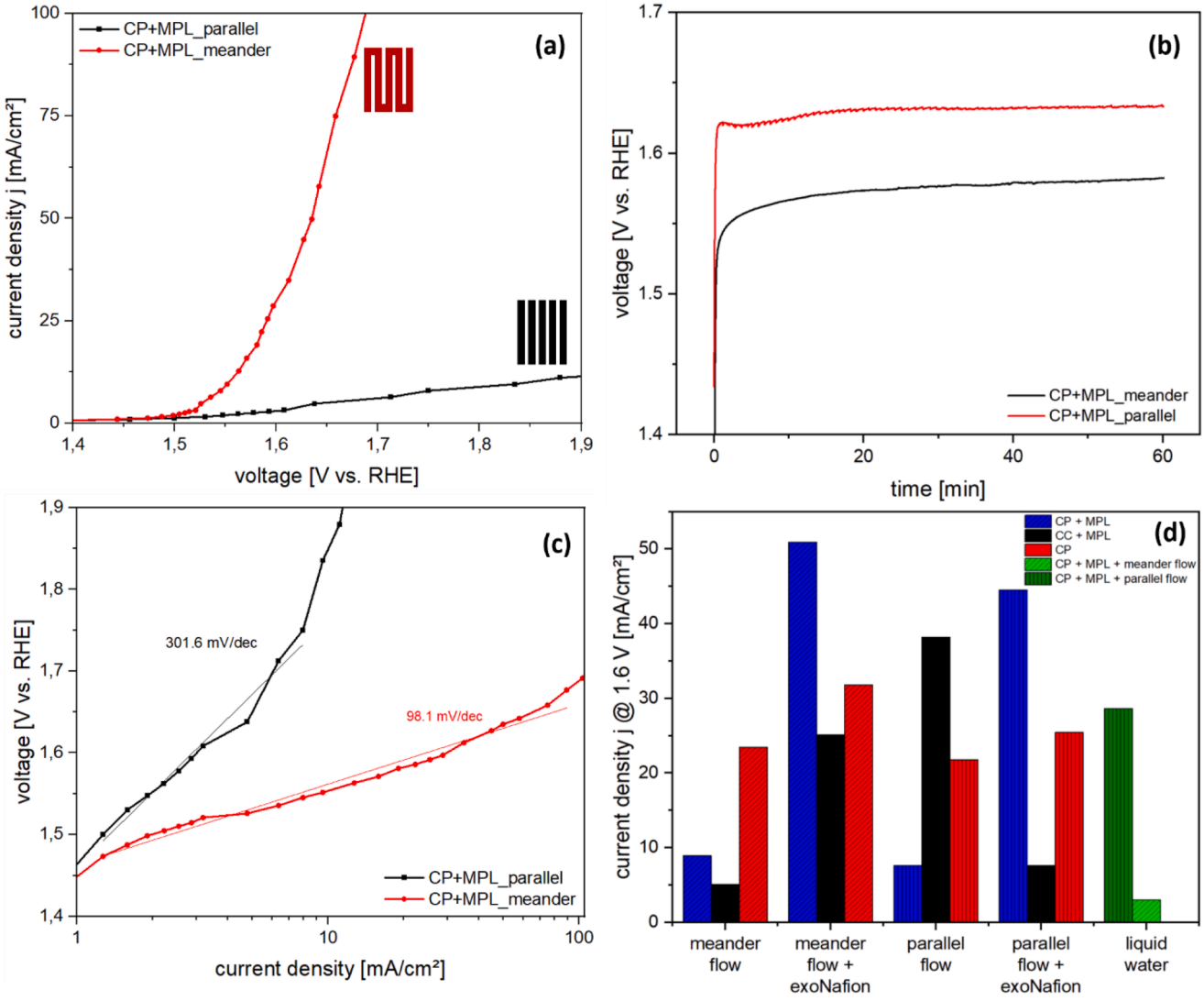

Fig. 5. (a) Polarization curves for OER on CP+MPL in meander flow field with exo-Nafion, N-117 membrane, 1 mg cm^{-2} Ir loading, 1 M H_2SO_4, water flow at 30 mL min^{-1}; (b) chronopotentiometry at 10 mA or 7.6 mA cm^{-2} (c) Tafel plot; and (d) electrochemical performance comparison of various GDEs at a cell potential of 1.6 V vs. RHE.

Table 2
GDE-performance in parallel or meander flow field with humidified N_2, 1 mg cm^{-2} Ir loading, 1 M H_2SO_4.

Flow field	Feed stream	GDL	Voltage at 7.6 mA cm^{-2} [V]	Overpotential [mV] at 7.6 mA cm^{-2}	Tafel slope [mV dec^{-1}]
parallel	humidified H_2O	CP+MPL	1.676	446	232.4
		CC+MPL	1.652	422	121.8
		CP	1.611	381	136.9
		CP+MPL+exoN	1.516	286	116.8
		CC+MPL+exoN	1.547	317	232.5
		CP+exoN	1.581	351	142.4
	liquid H_2O	CP+MPL+exoN	1.625	395	301.6
meander	humidified H_2O	CP+MPL	1.701	471	286.1
		CC+MPL	1.678	448	309.3
		CP	1.672	442	105.6
		CP+MPL+exoN	1.551	321	121.5
		CC+MPL+exoN	1.624	394	138.1
		CP+exoN	1.512	282	138.6
	liquid H_2O	CP+MPL+exoN	1.574	344	98.1

field but appear to have lower performance in the meandering flow field. In the case of the carbon paper, the meandering profile exhibited a small but significant and reproducible increase in performance compared to parallel flow. Due to the aforementioned performance profile for the carbon paper GDLs, the meandering profile should therefore be relied upon for these membrane-electrode assemblies (CP+MPL + exo-Nafion and N-117). Further experiments with liquid reactant feed showed a significantly lower overvoltage and better OER performance in the meandering field when compared to the parallel flow field. One crucial observation is that the current density at 1.6 V for the liquid reactant

feed in the meandering field is lower than that of the humidified gas reactant feed in the same GDE (i.e. CP+MPL with exo-Nafion) in both parallel and meandering flow field.

3.1.4. Catalyst properties at higher current densities in half-cells

In-situ XAS was applied to unravel the electrochemical changes during OER, as the catalysts are expected to behave very differently in the GDE set-up compared to their routine testing in RDE thin film design. The major difference between both procedures is that in GDE half-cell testing the catalysts are exposed to significantly higher currents, which in addition also cause the evolution and detachment of numerous gas bubbles from the surface during the reaction. This situation may result in non-negligible mechanical surface abrasion of the catalytic layer. A localised change of temperature on the GDE (i.e. the formation of local hot spots) might also occur. In order to visualise the changes at the various potentials and high currents, in-situ XAS of the Ir/VC-catalyst in the region from 11200 to 11250 eV (Ir L_3-edge) was performed. The in-situ investigation was carried out in the same electrolyte as above, however, in a slightly modified flow half-cell, especially designed to enable operando studies with ~3 ohms of resistance. A GDE exposure area of about ~30 mm^2 was employed, which can effectively sustain the required high current densities.

Fig. 6(a) inset shows the CV of Ir/VC measured with humidified N_2 in 1 M H_2SO_4 at a scan rate of 100 mV s^{-1} in the potential range of −0.1 V to 1.8 V. H_2 adsorption features on the Ir surface are not observed, which is indicative of blockage of the surface by strongly adsorbed SO_4^{2-} species. The redox features between 0.8 V and 1.1 V originate from the Ir^{III} / Ir^{IV} redox couple, which is known to form a matrix for reactive oxygen species acting as active sites for O_2 formation as the electrode potential reaches the OER onset region around 1.4 V [31]. X-ray absorption near edge structure (XANES) spectra recorded at the Ir L_3 edge at different polarization potentials from 0 V to 1.7 V at 0.1 V increments are depicted in Fig. 6(a). They exhibit a clear shift of the absorption edge towards higher energy values with the increase in potential and a more pronounced white-line, both features directly indicating the potential-dependent oxidation of Ir.

EXAFS fits for the first coordination shell of Ir nanoparticles (Fig. 6 (b)) were performed and showed the variation in the Ir-Ir and Ir-O coordination at different potentials. The coordination number (CN) changes for the metallic Ir-Ir and the Ir-O contribution fitted for different scattering paths are plotted in detail. Ir is clearly in its reduced state at the lower potentials (< 0.6 V). Following $CN_{Ir\text{-}Ir}$, a steady increase with potential is observed up to $E = 1.4$ V. Indeed, 1.4 V is the potential where the OER starts in the above CV, from there on, a decrease in the $CN_{Ir\text{-}Ir}$ is

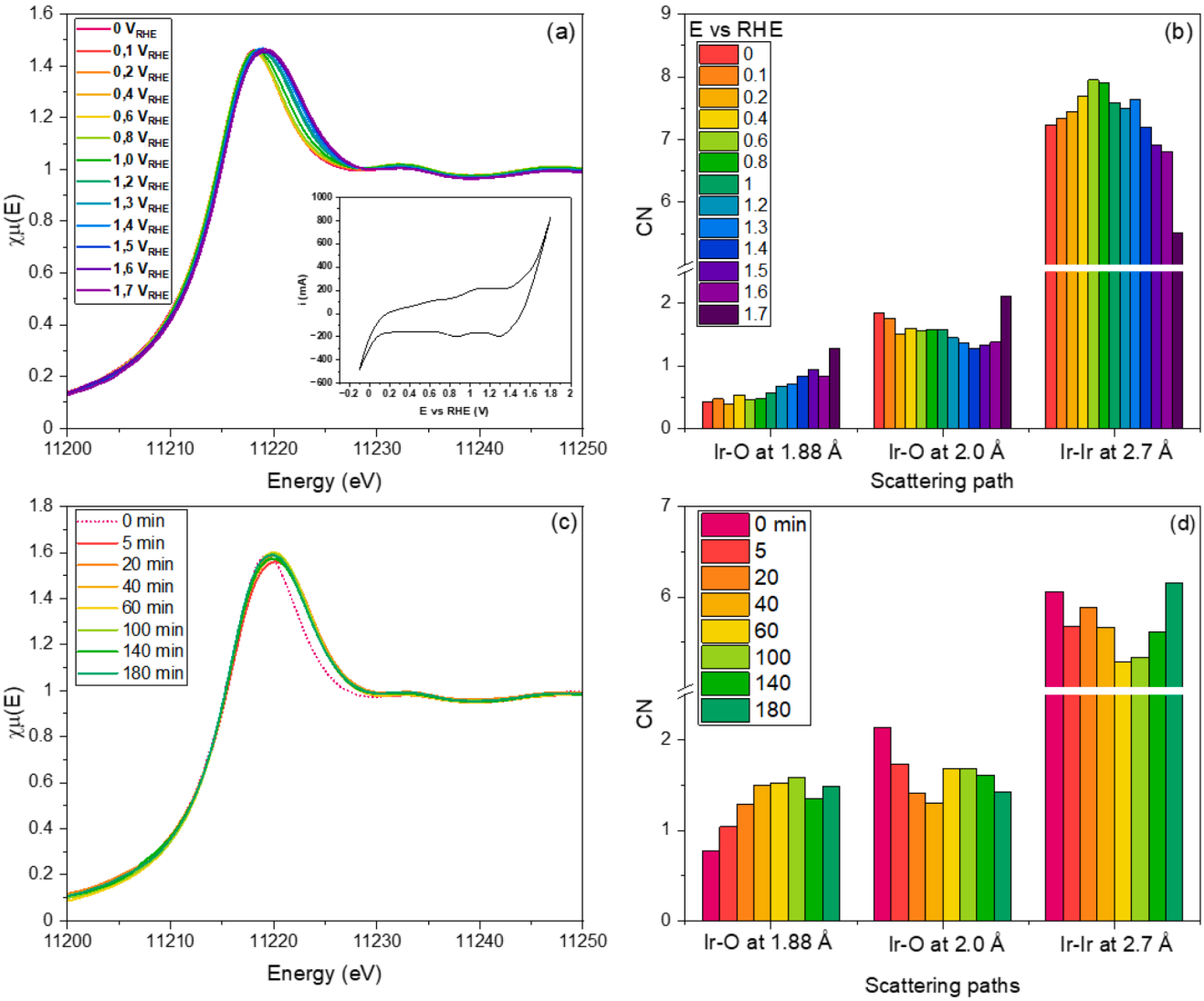

Fig. 6. (a) XANES of Ir L_3-edge, of Ir/VC in 1 M H_2SO_4 acquired at different potentials (inset) CV of Ir/VC in 1 M H_2SO_4; (b) Coordination numbers obtained from EXAFS fits from (a); (c) Time-dependent XANES of Ir L_3-edge obtained at 100 mA in 1 M H_2SO_4; (d) Coordination numbers (CN) obtained from EXAFS fits (c). The errors for CN and R fits were smaller than 10 %, and the R-factor was smaller than 15.

observed. At the same potential, a marginal increase in the $CN_{Ir\text{-}O}$ can be seen. In line with our observations, Siracusano et al. stated that the oxygen is released from the Ir lattice at such high potentials [39]. Our in-situ results thus might be interpreted by the Ir active sites using up reactive oxygen species to form the O-O bond, which are then released at the higher potentials. These changes are most dramatic at the potential of 1.7 V, at which point the evolution of oxygen was so high that it interfered with the acquisition of the XAS spectra (note: no further measurements could be obtained).

In-situ XAS studies were also conducted to follow and analyse the time-dependent changes of the catalyst subjected to the high current of 100 mA. Fig. 6(c) shows the XANES spectra of the GDE over a period of 3 h at a fixed current of 100 mA and Fig. 6(d) shows the corresponding EXAFS data. The Ir L_3-edge broadens from the spectrum at $t = 0$ min to $t = 5$ min, as soon as the GDE is subjected to the higher current, which then remains almost stable within the time frame studied. The $CN_{Ir\text{-}O}$ content in the first coordination shell increases at 1.88 Å over time. In contrast, $CN_{Ir\text{-}Ir}$ is first reduced, before it increases again (after 60 min). It has been reported in the literature that when the IrO_2 catalyst surface is exposed to conditions like potential cycling and potential holds in the high current region, alterations in oxidation state, change in Ir morphology and/or metal dissolution are possible [34,40]. OER mechanisms are known to be different at these higher potentials (correspondingly, higher current densities) and stronger Ir-Ir interactions have been observed by Czioska et al. using modulation excitation spectroscopy XAS [7]. The changes observed on the catalyst layer in the GDEs are more representative of the changes observed in realistic PEMWEs and vary greatly from what is seen in thin films on the RDE tips.

4. Conclusion

GDEs fabricated from three different GDL types, namely, CP, CP+MPL and CC+MPL, were utilised to study the effect of reactant flow field in a gas diffusion half-cell setup during the oxygen evolution reaction for water electrolysis with a polymer electrolyte membrane in acidic media. The presence of an exo-Nafion or ionomer layer and its effect on the onset of reaction, overpotential and high current densities in the flow fields were also studied systematically. It was observed that, 1) in the absence of the ionomer layer, the hydrophilic carbon paper (CP) had the best performance and was able to sustain high current densities irrespective of the flow field applied. The hydrophobic compressible and flexible carbon did not exhibit significant OER performance, irrespective of the flow field utilized. The hydrophobic carbon paper performance, on the other hand, depended quite heavily on the flow field used showing better performance in the parallel flow field; 2) in the presence of the ionomer layer on the GDEs, there was an overall lowering of the overpotential observed at 10 mA and an enhanced OER performance in both flow-field configurations with the exception of the hydrophobic compressible and flexible carbon in parallel flow field; 3) hydrophobic carbon paper with exo-Nafion with liquid flow through the meandering flow field demonstrated the lowest Tafel slope which suggests better OER kinetics with a liquid flow feed of the reactants; and lastly, 4) in-situ XAS studies on the catalyst in a GDE surface showed changes to the $CN_{Ir\text{-}Ir}$ and $CN_{Ir\text{-}O}$ during potential scans, which suggested activation of the catalytic centres, followed by their agglomeration and detachment during exposure to high currents for a longer time.

In addition to different gas diffusion layers, the influence of the membrane thickness remains to be studied in half-cell designs. A higher amount of flow channels can be considered to lead to a higher surface coverage of the electrode in laminar flow with increased half-cell performance. Variation in catalyst loading, ink preparation and coating techniques for the preparation of the catalyst layers also need to be optimized in such half-cells. In addition to material selection and set-up modification, durability should also be considered with respect to the application of half-cells in realistic environments. ASTs for the long-term stability of the GDEs at 25 °C and higher temperatures (>25 °C) need to be evaluated with regard to optimal performance in PEMWEs. A common benchmarked methodology and parameters for the gas diffusion half-cells will provide a faster throughput analysis of novel catalyst materials developed for OER in the future and allow for an easier comparison between different labs.

CRediT authorship contribution statement

Timon Elias Günther: Writing – review & editing, Writing – original draft, Methodology, Investigation, Formal analysis, Data curation. **Rameshwori Loukrakpam:** Writing – review & editing, Writing – original draft, Visualization, Validation, Supervision, Software, Methodology, Investigation, Formal analysis, Data curation. **Bruna Ferreira Gomes:** Writing – review & editing, Software, Methodology, Investigation, Formal analysis, Data curation. **Anouk Soisson:** Investigation, Formal analysis. **Melissa Moos:** Investigation. **Bui Duc Long Nguyen:** Investigation. **Sahil Shah:** Methodology. **Christina Roth:** Writing – review & editing, Writing – original draft, Visualization, Supervision, Resources, Project administration, Funding acquisition, Data curation.

Declaration of competing interest

The authors declare the following financial interests/personal relationships which may be considered as potential competing interests: Bruna Ferreira Gomes reports financial support was provided by Federal Ministry of Education and Research (BMBF). Rameshwori Loukrakpam reports administrative support and equipment, drugs, or supplies were provided by German Research Foundation. If there are other authors, they declare that they have no known competing financial interests or personal relationships that could have appeared to influence the work reported in this paper.

Acknowledgements

We would like to express our gratitude to Prof. Matthias Arenz from University of Bern for sharing the schematics of the half-cell setup and Lena Geiling for technical support with the SEM-EDX. Parts of this research were carried out at the experimental facilities at Petra III, DESY (Hamburg, Germany), a member of the Helmholtz Association HGF and we would like to thank Edmund Welter, Regina Biller and Sergej Wenz for the assistance provided while using the P65 beamline (beamtime was allocated for proposal I-20221072). The SEM-EDX (Ultra Zeiss Plus) at the Keylab Device Engineering in Bavarian Polymer Institute, University of Bayreuth is also acknowledged. We would further like to acknowledge Elitenetzwerk Bayern for their support in the study program "macromolecular science". This work is also funded by the Federal Ministry of Education and Research (BMBF) under Live XAS (Grant 05K22WC1) and HighHy (Grant 03SF0689B). We would like to express our gratitude to Dr. Michael Haumann and Prof. Holger Dau from Freie Universität Berlin for their invaluable assistance in the evaluation of XAS data and for providing access to the SimXLite software (for EXAFS fit) developed by the scientists at the KMC-3 beamline at BESSY-HZB. We gratefully acknowledge the support and funding by the German Research Foundation (DFG) within CRC 1585 (project number 492723217) for subproject A02.

Supplementary materials

Supplementary material associated with this article can be found, in the online version, at doi:10.1016/j.electacta.2024.145474.

Data availability

Data will be made available on request.

References

[1] M. Chatenet, B.G. Pollet, D.R. Dekel, F. Dionigi, J. Deseure, P. Millet, R.D. Braatz, M.Z. Bazant, M. Eikerling, I. Staffell, P. Balcombe, Y. Shao-Horn, H. Schäfer, Water electrolysis: from textbook knowledge to the latest scientific strategies and industrial developments, Chem. Soc. Rev. 51 (2022) 4583, https://doi.org/10.1039/D0CS01079K.

[2] S.S. Kumar, V. Himabindu, Hydrogen production by PEM water electrolysis – A review, Mater. Sci. Energy Technol. 2 (2019) 442–454, https://doi.org/10.1016/j.mset.2019.03.002.

[3] C. Qiu, Z. Xu, F.-Y. Chen, H. Wang, Anode engineering for proton exchange membrane water electrolyzers, ACS. Catal. 14 (2024) 921–954, https://doi.org/10.1021/acscatal.3c05162.

[4] C. Santoro, A. Lavacchi, P. Mustarelli, V. Di Noto, L. Elbaz, D.R. Dekel, F. Jaouen, What is next in anion-exchange membrane water electrolyzers? Bottlenecks, benefits, and future, ChemSusChem. 15 (2022) e202200027, https://doi.org/10.1002/cssc.202200027.

[5] Qi Feng, Xiao Zi Yuan, Gaoyang Liu, Bing Wei, Zhen Zhang, Hui Li, Haijiang Wang, A review of proton exchange membrane water electrolysis on degradation mechanisms and mitigation strategies, J. Power. Sources. 366 (2017) 33–55, https://doi.org/10.1016/j.jpowsour.2017.09.006.

[6] D. Abbott, D. Lebedev, K. Waltar, M. Povia, M. Nachtegaal, E. Fabbri, C. Copéret, T. Schmidt, Iridium oxide for the oxygen evolution reaction: correlation between particle size, morphology, and the surface hydroxo layer from operando XAS, Chem. Mater. 28 (2016) 6591–6604, https://doi.org/10.1021/acs.chemmater.6b02625, 18.

[7] S. Czioska, A. Boubnov, D. Escalera-López, J. Geppert, A. Zagalskaya, P. Röse, E. Saraci, V. Alexandrov, U. Krewer, S. Cherevko, J. Grunwaldt, Increased Ir–Ir interaction in iridium oxide during the oxygen evolution reaction at high potentials probed by operando spectroscopy, ACS Catal. 11 (2021) 10043–10057, https://doi.org/10.1021/acscatal.1c02074.

[8] M. Bernt, A. Siebel, H.A. Gasteiger, Analysis of voltage losses in PEM water electrolyzers with low platinum group metal loadings, J. Electrochem. Soc. 165 (5) (2018) F305–F314, https://doi.org/10.1149/2.0641805jes.

[9] Z. Fan, H. Yu, G. Jiang, D. Yao, S. Sun, B. Qin, Z. Shao, Durability testing of low-iridium PEM water electrolysis membrane electrode assemblies, Int. J. Hydrogen. Energy 47 (2022) 18963–18971, https://doi.org/10.1016/j.ijhydene.2022.04.114.

[10] M. Möckl, M.F. Ernst, M. Kornherr, F. Allebrod, M. Bernt, J. Byrknes, C. Eickes, C. Gebauer, A. Moskovtseva, H.A. Gasteiger, J. Electrochem. Soc. 169 (2022) 6, https://doi.org/10.1149/1945-7111/ac6d14.

[11] T. Wu, M. Sun, H.H. Wong, C.H. Chan, L. Lu, Q. Lu, B. Chen, B. Huang, Recent advances and strategies of electrocatalysts for large current density industrial hydrogen evolution reaction, Inorg. Chem. Front. 10 (2023) 4632–4649, https://doi.org/10.1039/D3QI00799E.

[12] C. Wang, L. Feng, Recent advances and perspectives of Ir-based anode catalysts in PEM water electrolysis, Energy Adv. 3 (2024) 14–29, https://doi.org/10.1039/D3YA00492A.

[13] J.K. Lee, G. Anderson, A.W. Tricker, F. Babbe, A. Madan, D.A. Cullen, J.D. Arregui-Mena, N. Danilovic, R. Mukundan, A.Z. Weber, X. Peng, Ionomer-free and recyclable porous-transport electrode for high-performing proton-exchange-membrane water electrolysis, Nat. Commun. 14 (2023) 4592, https://doi.org/10.1038/s41467-023-40375-x.

[14] C.M. Zalitis, D. Kramer, A.R. Kucernak, Electrocatalytic performance of fuel cell reactions at low catalyst loading and high mass transport, Phys. Chem. Chem. Phys. 15 (2013) 4329, https://doi.org/10.1039/C3CP44431G.

[15] A. Feidenhans'l, Y.N. Regmi, D.Xia C.Wei, J. Kibsgaard, L.A. King, Precious metal free hydrogen evolution catalyst design and application, Chem. Rev. 124 (2024) 5617–5667, https://doi.org/10.1021/acs.chemrev.3c00712, 9.

[16] B.A. Pinaud, A. Bonakdarpour, L. Daniel, J. Sharman, D.P. Wilkinson, Key considerations for high current fuel cell catalyst testing in an electrochemical half-cell (2017), J. Electrochem. Soc. (2017) 164 F321, https://doi.org/10.1149/2.0891704jes.

[17] K. Ehelebe, T. Ashraf, S. Hager, D. Seeberger, S. Thiele, S. Cherevko, Fuel cell catalyst layer evaluation using a gas diffusion electrode half-cell: oxygen reduction reaction on Fe-N-C in alkaline media, Electrochem. commun. 116 (2020) 106761, https://doi.org/10.1016/j.elecom.2020.106761.

[18] R. Loukrakpam, B.F. Gomes, T. Kottakat, C. Roth, A bird's eye perspective of the measurement of oxygen reduction reaction in gas diffusion electrode half-cell set-ups for Pt electrocatalysts in acidic media, J. Phys. Mater. 4 (2021) 044004, https://doi.org/10.1088/2515-7639/ac0319.

[19] R. Loukrakpam, B.F. Gomes, M. Prokop, C. Bauer, M. Kutter, F. Baier, R. Kempe, C. Roth, Challenges and limitations of accelerated stress testing in GDE half-cell set-ups, J. Power. Sources. 569 (2023) 232905, https://doi.org/10.1016/j.jpowsour.2023.232905.

[20] J. Schröder, J. Quinson, J.K. Mathiesen, J.J.K. Kirkensgaard, S. Alinejad, V. A. Mints, M. Arenz, K.M.O. Jensen, A New Approach to Probe the Degradation of Fuel Catalysts Under Realistic Conditions: combining Tests in a Gas Diffusion Electrode Setup with Small Angle X-Ray Scattering, J. Electrochem. Soc. 167 (2020) 134515, https://doi.org/10.26434/chemrxiv.12263804.v2.

[21] S. Alinejad, M. Inaba, J. Schröder, J. Du, J. Quinson, A. Zana, M. Arenz, Testing fuel cell catalysts under more realistic reaction conditions: accelerated stress tests in a gas diffusion electrode setup, J. Phys.: Energy 2 (2020) 024003, https://doi.org/10.1088/2515-7655/ab67e2.

[22] M. Inaba, A.W. Jensen, G.W. Sievers, M. Escudero-Escribano, A. Zana, M. Arenz, Benchmarking high surface area electrocatalysts in a gas diffusion electrode: measurement of oxygen reduction activities under realistic conditions, Energy Environ. Sci. 11 (2018) 988, https://doi.org/10.1039/C8EE00019K.

[23] J.H. Oh, G.H. Han, H. Kim, H.W. Jang, H.S. Park, S.Y. Kim, S.H. Ahn, Activity and stability of Ir-based gas diffusion electrode for proton exchange membrane water electrolyzer, Chemical Engineering Journal 420 (2021) 127696, https://doi.org/10.1016/j.cej.2020.127696.

[24] J. Schröder, V.A. Mints, A. Bornet, E. Berner, M. Fathi Tovini, J. Quinson, G.K. H. Wiberg, F. Bizzotto, H.A. El-Sayed, M. Arenz, The gas diffusion electrode setup as straightforward testing device for proton exchange membrane water electrolyzer catalysts, JACS. Au 1 (2021) 247–251, https://doi.org/10.1021/jacsau.1c00015.

[25] F.H. Roenning, A. Roy, D.S. Aaron, M.M. Mench, Mass transport limitations in polymer electrolyte water electrolyzers using spatially-resolved current measurement, J. Power. Sources. 542 (2022) 231749, https://doi.org/10.1016/j.jpowsour.2022.231749.

[26] H. Zhou, K. Meng, B. Chen, Two-phase flow evolution and bubble transport characteristics in flow field of proton exchange membrane water electrolyzer based on volume of fluid-coupled electrochemical method, J. Clean. Prod. 425 (2023) 138988, https://doi.org/10.1016/j.jclepro.2023.138988.

[27] R. Yang, J. Yesuraj, K. Kim, Effect of Flow Channel Shape and Operating Temperature on the Performance of a Proton Exchange Membrane Electrolyzer Cell, Energy Fuels. 37 (2023) 12178–12191, https://doi.org/10.1021/acs.energyfuels.3c01629.

[28] P.C. Jiménez, G.K.H. Wiberg, G.W. Sievers, V. Brüser, M. Arenz, Bridging the gap between basic research and application: a half-cell setup for high current density measurements of Ir-based oxygen evolution reaction catalysts on porous transport electrodes, J. Mater. Chem. A 11 (2023) 20129, https://doi.org/10.1039/D3TA04136K.

[29] S.K. Mondal, D. Kar, M Das, A comparative kinetic study of iridium(III) catalysis in cerium(IV) oxidation of dioxane in aqueous sulfuric acid and perchloric acid media, Transition Metal Chemistry 23 (1998) 593–598, https://doi.org/10.1023/A:1006992905510.

[30] B. Ravel, M. Newville, ARTEMIS ATHENA, HEPHAESTUS: data analysis for X-ray absorption spectroscopy using IFEFFIT, J. Synchrotron. Radiat. 12 (2005) 537–541, https://doi.org/10.1107/S0909049505012719.

[31] K. Ehelebe, N. Schmitt, G. Sievers, A.W. Jensen, A. Hrnjić, P. Collantes Jiménez, P. Kaiser, M. Geuß, Y.-P. Ku, P. Jovanovič, K.J.J. Mayrhofer, B. Etzold, N. Hodnik, M. Escudero-Escribano, M. Arenz, S. Cherevko, Benchmarking fuel cell electrocatalysts using gas diffusion electrodes: inter-lab comparison and best practices, ACS Energy Lett. 7 (2022) 816–826, https://doi.org/10.1021/acsenergylett.1c02659.

[32] M. Carmo, D.L. Fritz, J. Mergel, D. Stolten, A comprehensive review on PEM water electrolysis, Int. J. Hydrogen. Energy 38 (2013) 4901–4934, https://doi.org/10.1016/j.ijhydene.2013.01.151.

[33] H. Butsch, C. Roth, D. Ritzingerm G. Hoogers, A. Bock, Spatially resolved contact pressure and contact resistance measurements at the gas diffusion layer: a tool for PEM Fuel Cell Development, J. Electrochem. Soc. 159 (2012) 6. https://iopscience.iop.org/article/10.1149/2.054206jes.

[34] V. Pfeifer, T.E. Jones, J.J. Velasco Vélez, R. Arrigo, S. Piccinin, M. Hävecker, A. Knop-Gericke, R. Schlögl, In situ observation of reactive oxygen species forming on oxygen-evolving iridium surfaces, Chem. Sci. 8 (2017) 2143, https://doi.org/10.1039/C6SC04622C.

[35] Freudenberg performance materials, Freudenberg gas diffusion layers technical data (2024), https://fuelcellcomponents.freudenberg-pm.com/-/media/Files/fuelcellcomponents,-d-,freudenbergpm,-d-,com/FPM_technical_data_sheet_gdl_ENG_2018-07-04.pdf.

[36] R. Schweiss, C. Meiser, T. Damjanovic, I. Galbati, N. Haak, SGL Carbon group, White paper sigracet gas diffusion layer (2024), https://www.fuelcellstore.com/spec-sheets/sigracet-gdl-white-paper-new-generation.pdf.

[37] X. Duan, X. Xiang, J. Chen, A. Zhou, J. Xiao, J. Wen, S. Wang, Numerical simulation and multi-objective optimization on flow performance of novel alkaline water electrolyzer, Int. J. Hydrogen. Energy 55 (2024) 1505–1513, https://doi.org/10.1016/j.ijhydene.2023.11.176.

[38] T. Wang, J. Wang, P. Wang, Z. Ren, X. Yan, W. Wang, W. Guo, Plate structure design guideline for commercial alkaline water electrolyzers (AWEs) with improved liquid flow uniformity: multi-scale quantitative criteria and experimental validation, Int. J. Hydrogen. Energy 49 (2024) 907–924, https://doi.org/10.1016/j.ijhydene.2023.09.315.

[39] S. Siracusano, N. Hodnik, P. Jovanovic, F. Ruiz.Zepeda, M. Sala, V. Baglio, A. S. Aricò, New insights into the stability of a high performance nanostructured catalyst for sustainable water electrolysis, Nano Energy 40 (2018) 618–632, https://doi.org/10.1016/j.nanoen.2017.09.014.

[40] N. Diklic, A. Beard, J. Herranz, A. Heinritz, T. Cen, S. Garbe, D.F. Abbott, M. Povia, T.J. Schmidt, Breaking down the performance losses in O_2-evolution stability tests of IrO_2-based electrocatalysts, J. Electrochem. Soc. 170 (2023) 074503. https://iopscience.iop.org/article/10.1149/1945-7111/ace741.